

## 250- and 9.5-GHz EPR Studies of an Electride and Two Alkalides

Dae Ho Shin and James L. Dye\*

*Department of Chemistry and Center for Fundamental Materials Research, Michigan State University, East Lansing, Michigan 48824*

David E. Budil, Keith A. Earle, and Jack H. Freed

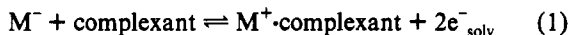
*Baker Laboratory of Chemistry, Cornell University, Ithaca, New York 14853*

Received: October 9, 1992

The EPR spectra of polycrystalline samples of  $\text{Cs}^+(\text{18C6})_2\text{X}^-$ , in which  $\text{X}^- = \text{e}^-$ ,  $\text{Na}^-$ , or  $\text{Cs}^-$ , were studied at both X-band (9 GHz) and at 250 GHz. The high frequency affords much better  $g$ -factor resolution and reveals at least two types of asymmetric electron sites in each of these compounds. The defect electrons detected in the alkalides  $\text{Cs}^+(\text{18C6})_2\text{Na}^-$  and  $\text{Cs}^+(\text{18C6})_2\text{Cs}^-$  appear to be located at isolated centers in the crystal lattice with the strongest signal originating from electrons trapped at anion vacancies. These species exhibit broadening due to unresolved superhyperfine interactions at the periphery of the trapping site. In contrast, the X-band spectra of the two-electron sites in the electride appear to be exchange-narrowed, indicating that the electron spins have some degree of mobility within the crystal lattice. Comparison of the 9- and 250-GHz spectra of the electride places an upper bound of about  $1 \times 10^7 \text{ s}^{-1}$  on the rate of spin exchange. The temperature and saturation behavior of the electride at X-band are consistent with the "F-center" model, in which electrons serve to balance the charge of the complexed cations, with the center of charge of each electron at an anionic site. The strongest signal in  $\text{Cs}^+(\text{18C6})_2\text{e}^-$  has nearly the same  $g$ -anisotropy as one of the signals from the isostructural sodide,  $\text{Cs}^+(\text{18C6})_2\text{Na}^-$ , indicating that at least one of the electron-trapping sites detected in the two crystal lattices is the same. The temperature dependence of the two EPR signals from  $\text{Cs}^+(\text{18C6})_2\text{Cs}^-$  at X-band suggests an activated process that populates two types of unpaired electron sites from a common spin-paired precursor.

## Introduction

Since the isolation of the first salt of an alkali metal anion in 1974,<sup>1,2</sup> many of the physical properties of alkalides and electrides have been characterized. Polycrystalline alkalides and electrides are synthesized from solutions that contain the alkali cation, complexed by a crown ether, cryptand, or aza analogue, and an equal concentration of either alkali metal anions or solvated electrons. However, no solution contains exclusively  $\text{M}^-$  or  $\text{e}^-$ . The concentration of these two species is governed by the dissociation equilibrium



Consequently, some electrons are always trapped in crystalline alkalides. The concentration of trapped electrons depends on the synthetic method used. For example, slow crystallization and an excess of alkali metal tend to produce lower concentrations of trapped electrons.

A major goal of EPR studies of alkalides and electrides is to determine the nature of the electron trapping site(s) and the degree of overlap of the trapped electron wavefunction with nearby nuclei. In most electrides studied to date, the concentrations and exchange rates are so high that only a single exchange-narrowed EPR line is seen at X-band. Electron trapping in the analogous alkalides thus provides an opportunity to study the nature of the trapped electrons in the absence of exchange.

The wavefunction of an electron trapped in an alkalide can have a significant spatial extent, which leads to hyperfine interactions with nearby nuclei. The spin density of the trapped electron at the alkali cation changes with the structure of the anionic site for both alkalides and electrides. The most obvious indication of this electronic charge distribution is the EPR line broadening and hyperfine splitting due to Fermi contact and/or

electron nuclear dipolar interaction. Generally, when the cation is well-shielded within a cryptand cage or in a sandwich crown ether complex, the contact electron density at the cation due to the trapped electron is small.<sup>3</sup> By contrast, if the alkali cation is exposed to the anionic site, as in a one-to-one crown ether complex, or when a methylated aza-crown is used,<sup>3-5</sup> the contact electron density of the trapped electron at the cation can be large. For the former case, no hyperfine splitting is observed due to the low contact electron density at the cation and the interaction of the electron with a number of nuclei. The latter case shows hyperfine splitting due to a relatively strong interaction between each trapped electron and a single cation.

The X-band EPR spectrum of  $\text{Cs}^+(\text{18C6})_2\text{Na}^-$  showed at least two signals, a strong broad line and a narrow central line with much smaller integrated intensity.<sup>3</sup> The intensity ratio of the two peaks depended on the synthesis. No resolved hyperfine splitting or  $g$ -anisotropy were observed; the line broadening could have resulted either from superhyperfine coupling to a number of surrounding nuclei or to a distribution of  $g$ -values.<sup>3</sup> The use of high-field EPR in the present study was initiated to address this uncertainty, given its unique capability to resolve spectra from species with very closely spaced  $g$ -values.

Previous EPR studies of  $\text{Cs}^+(\text{18C6})_2\text{Cs}^-$  showed the presence of at least two electron trapping sites with complex temperature behavior.<sup>6</sup> Rotation of a single crystal demonstrated the presence of  $g$ -anisotropy. No identification of the sites responsible for the EPR peaks was made at the time.

*Electrides* are crystalline compounds in which trapped or itinerant electrons are present in amounts equal to those of the complexed cations.<sup>6-14</sup> Thus, electrons serve in place of the anions of alkalides to balance the cationic charge. The physical properties of electrides and their structural similarity to corresponding alkalides strongly suggest that electrons are trapped stoichiometrically at all of the anionic sites. The crystal structures of electrides show large vacancies at the locations of the anionic

\* To whom correspondence should be addressed.

sites, but the trapped electrons cannot be directly detected because of the low electron density.

Previous studies of the X-band EPR spectra of  $\text{Cs}^+(\text{18C6})_2\text{e}^-$  at temperatures as low as 2.9 K showed only a single narrow (0.5 G) line whose width was independent of temperature. The lineshape became Dysonian at higher temperatures, indicating high microwave conductivity. The activation energy for this conductivity was only 0.05 eV, much lower than the apparent dc activation energy of 0.45 eV. These results indicated rapid electron exchange, even at the lowest temperatures measured.<sup>6</sup>

Recent dc and ac powder conductivity studies of electrides<sup>14</sup> have revealed that contamination of the electride  $\text{Cs}^+(\text{18C6})_2\text{e}^-$  with small amounts of  $\text{Cs}^-$  drastically affects the conductivity, increasing the electronic contribution by several orders of magnitude. Apparently, the presence of small amounts of excess cesium provides a mechanism for electron migration and exchange that is not present in the pure electride.

Recent magnetic susceptibility studies<sup>16</sup> of  $\text{Cs}^+(\text{18C6})_2\text{e}^-$  have brought to light an additional complication that occurs with this electride. Carefully crystallized samples that have the published crystal structure<sup>8</sup> are antiferromagnetic with a Néel temperature of  $\sim 50$  K and a high-temperature slope that accounts for all the spins, provided the temperature is maintained below about 230 K at all times from crystallization to measurement. Upon raising the temperature in the SQUID above 230 K an irreversible change occurs in which the spin count remains the same, but the antiferromagnetic transition is replaced by an inflection. This behavior contrasts with previous results<sup>6</sup> on samples that presumably contained some excess cesium and that showed Curie-Weiss behavior with a Weiss constant of only  $-1.5$  K.

All of these results show that the properties of  $\text{Cs}^+(\text{18C6})_2\text{e}^-$  are critically dependent upon the method of synthesis and the thermal history of the sample. The electride of known crystal structure has only a single type of anionic site and shows antiferromagnetic interactions among the electrons. It converts to a more complex form at higher temperatures that may be responsible for the two closely spaced <sup>133</sup>Cs NMR peaks whose relative intensities are temperature dependent.<sup>17</sup> The presence of small amounts of excess cesium has a dramatic effect on the conductivity, susceptibility, and EPR spectra of this electride.

The present study of the X-band and 250-GHz EPR spectra of three compounds that contain the complexed cesium cation,  $\text{Cs}^+(\text{18C6})_2$ , was initiated in an attempt to separate the effects of multiple trapping sites, hyperfine broadening, and *g*-anisotropy on the EPR spectra of  $\text{Cs}^+(\text{18C6})_2\text{e}^-$ ,  $\text{Cs}^+(\text{18C6})_2\text{Na}^-$ , and  $\text{Cs}^+(\text{18C6})_2\text{Cs}^-$ .

## Experimental Methods

**Sample Preparation.** The sample preparation methods used for X-band EPR studies have been described elsewhere.<sup>18</sup> In synthesizing the electride, care was taken to prevent inclusion of excess cesium by using excess complexant during crystallization. For 250-GHz EPR studies, polycrystalline samples of  $\text{Cs}^+(\text{18C6})_2\text{Na}^-$  and  $\text{Cs}^+(\text{18C6})_2\text{e}^-$  and single crystals of  $\text{Cs}^+(\text{18C6})_2\text{Cs}^-$  were ground with a mortar and pestle below  $-50$  °C under a dry nitrogen atmosphere in a glovebag. The samples for the high-field studies were loaded into the sample holder described below under cold nitrogen and then sealed with a Mylar film. A larger sample volume could be used than at X-band. An amount of sample was used that filled about half of the sample holder.

**Sample Holder.** The sample holder for the 250-GHz spectrometer has been previously described.<sup>19</sup> It is conical in shape with a 10-mm-deep cylindrical sample well 3.8 mm in diameter. Poly(methylpentene) (TPX), Teflon, and Z-cut quartz had been previously used as window materials for the sample holder, because of their low absorbance at 1.2 mm (250 GHz). However, these materials could not be used for the present study. Teflon was

avoided because of its potential to react with our samples, and it proved impossible to construct a sample holder with a quartz window for use near liquid nitrogen temperature because of differential contraction of the sample holder material and the window. Rexolite (cross-linked polystyrene from General Electric) was chosen as the best compromise between transmission at 250 GHz and stability with respect to the solvent and samples. Even though the windows had some tool marks, their optical performance was not compromised because the surfaces were flat to better than  $\lambda/8$ . The samples were stored under liquid nitrogen in a Dewar.

**Instrumentation.** X-band EPR spectra were obtained with a Bruker 200D EPR spectrometer with a TE<sub>102</sub> rectangular cavity. An ER350 NMR gaussmeter was used to measure the field to  $\pm 1$ -mG resolution. The microwave frequency was measured to 0.01 MHz with an HP5245 frequency counter. The *g*-values of X-band spectra were obtained directly from the magnetic field strength and the microwave frequency. The temperature was controlled by adjusting the flow rate of cold nitrogen.

The 250-GHz EPR spectrometer developed by Lynch et al. in the laboratory of Freed<sup>19</sup> was used to obtain the high-frequency EPR spectra. The FIR source was a Millitech Corp. PLS-3F phase-locked solid-state source that delivered 3–5 mW at 250 GHz (via a WR-4 waveguide). A semiconfocal Fabry-Perot resonator was used for the sample cavity, which was tuned by controlling the distance between two mirrors. The main magnetic field was provided by a superconducting solenoid maintained in the persistent mode at about 89 kG. The field was swept by using a second superconducting solenoid driven by an HP6032A power supply that provided point-to-point resolution of 0.188 G. The combined field homogeneity of both main and sweep coils was about  $3 \times 10^{-6}$  over a 10-mm-diameter spherical volume. EPR spectra were obtained in the standard way by modulating the field at 65 kHz with a small solenoid placed around the sample in the warm bore of the magnet Dewar and measuring the first-derivative signal with a lock-in amplifier. The temperature could be controlled to within about 1° over the range 150–230 K by using a heater and regulating the flow rate of cold nitrogen gas. The magnetic field was calibrated with a <sup>2</sup>H NMR gaussmeter (Sentec Model 1101). The field calibration affords a *relative g*-value accuracy on the order of  $10^{-6}$ ; however, the average *g*-values measured at high field were calibrated to the X-band spectra, so that the *absolute* accuracy of the *g*-values is only about  $5 \times 10^{-5}$ .

**Spectral Simulation.** Experimental EPR spectra were simulated by using first-order energies from the spin Hamiltonian

$$H_S = \beta_e S g B_0 + \sum_i^n S A_i I_i \quad (2)$$

For the spectra simulated in this work, no resolved hyperfine interactions were observed; instead, a distribution of unresolved hyperfine interactions corresponding to the second term in eq (2) was modeled by using an orientation-dependent linewidth when necessary. Integration over angular distribution to give the EPR "powder pattern" was carried out with the aid of a Curtis-Cleenshaw-Romberg numerical integration.<sup>20</sup>

## Results and Discussion

$\text{Cs}^+(\text{18C6})_2\text{e}^-$ . X-ray crystallography has shown that the compounds  $\text{Cs}^+(\text{18C6})_2\text{e}^-$  and  $\text{Cs}^+(\text{18C6})_2\text{Na}^-$  are isostructural and that the metal cation is rather isolated from the metal anion or trapped electron in the crystal structure.<sup>8</sup> Presumably, most of the electrons in these compounds are trapped at anionic vacancies, although the presence of interstitial electrons and ions cannot be ruled out. Cesium-free  $\text{Cs}^+(\text{18C6})_2\text{e}^-$  appears to be primarily an ionic conductor with an activation energy of about 1.1 eV; the conduction mechanism is probably closely related to

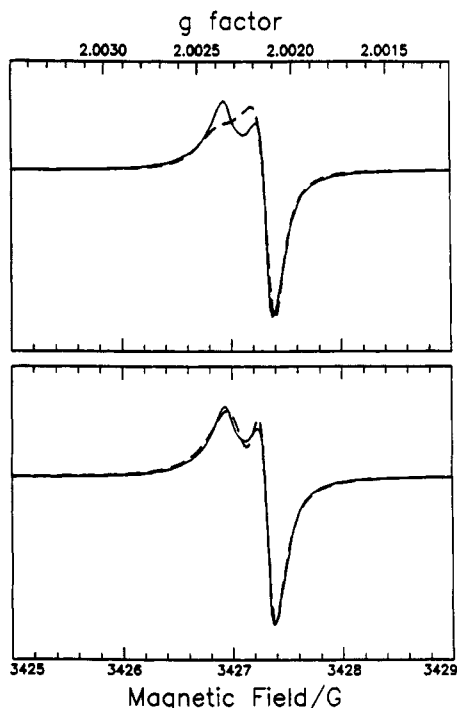


**Figure 1.** (A, Top) Experimental X-band EPR spectrum of  $\text{Cs}^+(18\text{C}6)_2\text{e}^-$  at 143 K (solid line) with spectral simulation for a single site with axial  $g$ -anisotropy (dotted line). (B, Bottom) Same experimental spectrum with simulation based on two superimposed Lorentzians (dashed line) as specified in the text.

that of  $\text{Cs}^+(15\text{C}5)_2\text{e}^-$ .<sup>15</sup> The thermal history of these samples was similar to that of the high-temperature form used in susceptibility studies.<sup>16</sup>

Figure 1 shows the X-band EPR spectrum of ceside-free  $\text{Cs}^+(18\text{C}6)_2\text{e}^-$  at 143 K. The spectrum differs qualitatively from spectra previously obtained from this compound in that it does not exhibit the Dysonian line shape indicative of high microwave conductivity.<sup>6</sup> However, the interpretation of the X-band spectrum alone remains somewhat ambiguous. Superficially, the spectrum has the appearance of a single species with negligible hyperfine splittings ( $<0.06$  MHz) and axially symmetric  $g$ -anisotropy with  $g_{\perp} = 2.0021$  and  $g_{\parallel} = 2.0024$ . However, attempts to simulate the spectrum under this assumption met with only limited success, as shown by the dashed line in Figure 1A. The least-squares spectral simulation using the  $g$ -values noted above and a Lorentzian line shape required an orientation-dependent linewidth tensor with  $(\Delta H_{pp})_{\perp} = 0.31$  G and  $(\Delta H_{pp})_{\parallel} = 0.15$  G. Alternatively, the spectrum may be interpreted as the superposition of two nearly isotropic Lorentzian lines centered at  $g = 2.0027$  and  $2.00214$  with derivative peak-to-peak linewidths of 0.31 and 0.15 G, respectively, and relative integrated intensities of 1.9:1. This model provides a significantly better fit to the experimental line shape as shown by the dashed line in Figure 1B.

The 250-GHz spectrum of  $\text{Cs}^+(18\text{C}6)_2\text{e}^-$  taken at 158 K is shown in Figure 2. At sufficiently low modulation amplitude, the spectrum exhibited some irregular fine structure between the major broad peaks. This effect has been observed in other high-field studies of polycrystalline solid-state materials<sup>21</sup> and may be attributed to the presence of a few microcrystals that had not been ground finely enough to yield a truly isotropic distribution of sample orientations. The polycrystalline effects do not significantly distort the overall line shape shown in Figure 2, but they do provide an important indication that the homogeneous linewidth of the signal is much smaller than the linewidth due to  $g$ -anisotropy at the high field.

The high-frequency spectrum of  $\text{Cs}^+(18\text{C}6)_2\text{e}^-$  is most consistent with the presence of two electron-trapping sites in the crystal. The splitting between the extreme features of the

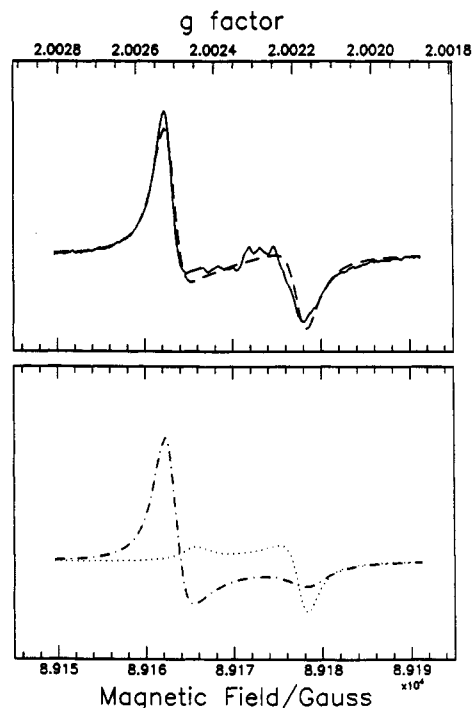


**Figure 2.** (A, Top) Experimental 250-GHz EPR spectrum of  $\text{Cs}^+(18\text{C}6)_2\text{e}^-$  at 158 K (solid line) and least-squares spectral simulation for two sites with  $g$ -anisotropy (dashed line). (B, Bottom) Individual spectra for the sum spectrum shown in (A). Parameters used for the simulations appear in Table I.

spectrum does scale approximately with frequency as one might expect for a single species with  $g$ -anisotropy. However, the details of the high-field spectral line shape—in particular, the sharp, intense feature on the low-field side of the spectrum—could not be successfully simulated by using a single component with  $g_{\parallel} > g_{\perp}$ . Reasonable agreement could only be achieved by including a second component with axial or nearly axial symmetry and  $g_{\parallel} < g_{\perp}$ , as shown in Figure 2. The relative intensities of the signals with  $g_{\parallel} > g_{\perp}$  and  $g_{\parallel} < g_{\perp}$  are about 1:3.0. The magnetic parameters used for the simulations shown in Figure 2 are given in Table I.

In combination, the spectra obtained at X-band and at 250 GHz suggest that the trapped electrons in  $\text{Cs}^+(18\text{C}6)_2\text{e}^-$  are somewhat mobile or undergo a weak spin exchange interaction. The  $g$ -anisotropies measured at 250 GHz predict a slightly wider spectrum than is actually observed at X-band. This could come about if the  $g$ -anisotropy is averaged at X-band by spin exchange or by hopping of the electron spins between different trapping sites in the crystal lattice. At 250 GHz, the spectral extent due to  $g$ -anisotropy is apparently too large to be completely averaged by such motion. The spectral extent of the 250-GHz data thus places an upper limit on the exchange rate of about  $10^7$  s<sup>-1</sup>.

The temperature dependences of the linewidth, line shape, and intensity of the EPR signal were studied at X-band and the temperature dependences of the linewidth and line shape were also studied at 250 GHz. The high-frequency spectrum exhibited a slight temperature dependence, with the overall width of the spectrum increasing from 15.3 to 19 G as the temperature was decreased from 230 to 134 K. This effect might be due to a physical change in the size of the electron-trapping cavity with temperature, or it could reflect a change in the rate of electron hopping that alters the effective averaged  $g$ -tensors as a function of temperature.

The integrated intensity of the X-band EPR spectrum is plotted as a function of inverse temperature in Figure 3 and is linear with inverse temperature, but with an appreciable positive intercept at  $1/T = 0$ . This behavior indicates that the trapped electrons are not involved in *substantial* spin-pairing in this temperature

**TABLE I: Magnetic Parameters of Trapped Electron Centers in  $\text{Cs}^+(\text{18C6})_2\text{e}^-$ ,  $\text{Cs}^+(\text{18C6})_2\text{Na}^-$ , and  $\text{Cs}^+(\text{18C6})_2\text{Cs}^-$  Determined from 250-GHz EPR Spectroscopy of Polycrystalline Samples**

	$\text{Cs}^+(\text{18C6})_2\text{e}^-$		$\text{Cs}^+(\text{18C6})_2\text{Na}^-$		$\text{Cs}^+(\text{18C6})_2\text{Cs}^-$	
	site 1	site 2	site 1	site 2	site 1	site 2
$g_1^{a,b}$	2.002 523	2.002 457	2.002 587	2.002 385	2.002 675	2.002 773
$g_2$	2.002 523	2.002 187	2.002 545	2.002 320	2.002 642	2.002 347
$g_3$	2.002 163	2.002 187	2.002 275	2.002 175	2.002 368	2.002 332
$(\Delta H_{pp})_1^c$	1.8	2.0	1.5	1.1	0.80	0.85
$(\Delta H_{pp})_2$	1.8	1.8	1.5	1.8	0.80	1.0
$(\Delta H_{pp})_3$	2.8	1.8	2.5	1.8	1.5	1.0
rel int	3.0	1	3.2	1	1.0	1

<sup>a</sup> Reported  $g$ -values have estimated relative uncertainties of  $\pm 3 \times 10^{-6}$  and estimated absolute uncertainties of  $5 \times 10^{-5}$ . <sup>b</sup> Reported  $g$ -tensor principal values  $g_1$ ,  $g_2$ , and  $g_3$  do not refer to a specific axis system and are only arranged according to decreasing value. <sup>c</sup> Linewidths refer to the derivative peak-to-peak width of a Lorentzian lineshape, in gauss, with estimated uncertainties of  $\pm 0.1$  G.

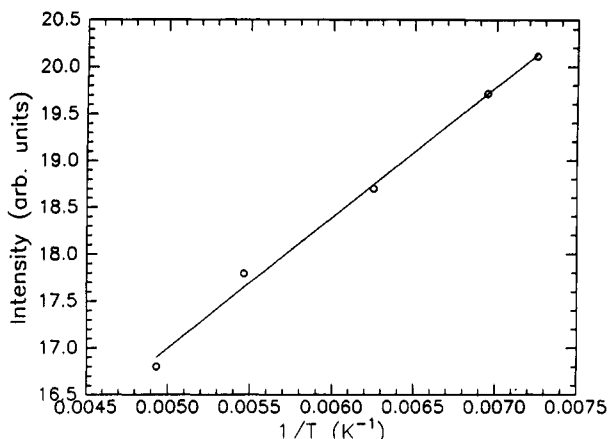


**Figure 3.** Temperature dependence of the intensity of the X-band EPR spectrum of  $\text{Cs}^+(\text{18C6})_2\text{e}^-$ .

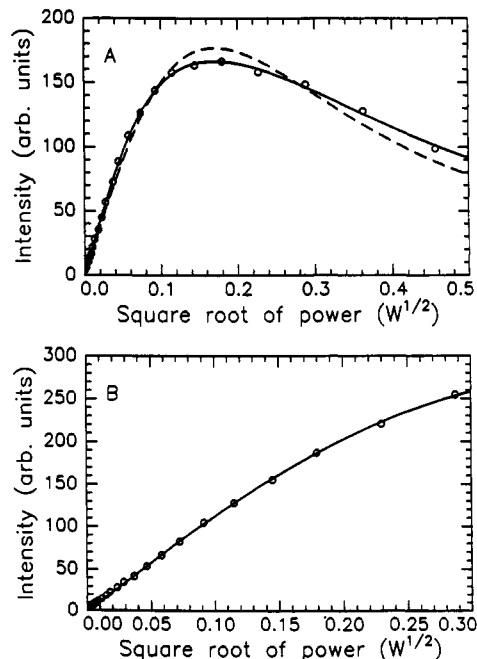


**Figure 4.** Saturation curves measured at X-band for (A)  $\text{Cs}^+(\text{18C6})_2\text{e}^-$  at 143 K and (B)  $\text{Cs}^+(\text{18C6})_2\text{Na}^-$  at 148 K. Data are plotted as derivative peak-to-peak intensity of the spectrum vs applied microwave power.

range, although the non-zero intercept suggests some electron-pair dissociation at the higher temperatures.

A microwave power saturation study of  $\text{Cs}^+(\text{18C6})_2\text{e}^-$  carried out at X-band also supports the conclusion that two distinct electron-trapping sites with different spin relaxation properties are present in this crystal lattice. Figure 4A shows the measured peak-to-peak amplitude of the signal as a function of microwave power. The data were fit by using a local implementation<sup>22</sup> of

the Marquardt–Levenberg nonlinear least-squares minimization<sup>23</sup> to the equation

$$y'_m = y'^0_m \frac{B_1}{(1 + B_1^2 \gamma_e^2 T_1 T_2)^{3/2}} \quad (3)$$

where  $y'_m$  is the peak-to-peak amplitude of the signal and  $y'^0_m = y'_m/B_1$  in the limit  $B_1 = 0$ .<sup>24</sup> The best fit of a theoretical saturation curve for the derivative of a single Lorentzian peak deviates appreciably from the experimental data, as shown by the dashed line in Figure 4a. Significantly better agreement resulted when two saturation curves of the form given by eq 3 were added together, as shown by the solid line in Figure 4A.

The conclusion that the X-band spectrum consists of two exchange-narrowed lines is also supported by results obtained in our attempts to measure electron spin-echo envelope modulation (ESEEM) from  $\text{Cs}^+(\text{18C6})_2\text{e}^-$ . Although this sample produces a strong free induction decay signal corresponding to a rather long value of  $T_2$ , no spin-echo could be observed. This result is most consistent with the presence of two closely spaced homogeneous lines, since a single electron site with resolvable  $g$ -anisotropy in the cw spectrum should be inhomogeneous enough to produce an echo.

The results are all consistent with the assumption that most of the unpaired electrons in  $\text{Cs}^+(\text{18C6})_2\text{e}^-$  are localized in the anionic cavities. The average  $g$ -value of the trapped electrons in  $\text{Cs}^+(\text{18C6})_2\text{e}^-$  is close to the free electron  $g$ -value, and the anisotropy is very small, indicating that the electrons experience only very small spin-orbit interactions. This result is consistent with the crystal structure of  $\text{Cs}^+(\text{18C6})_2\text{e}^-$ ,<sup>8</sup> in which the anion cavity is rather isolated from the cations by the complexant molecules, so that spin-orbit coupling centered on the heavy  $\text{Cs}^+$  ions can make only a small contribution to the  $g$ -anisotropy. The presence of two trapping sites is consistent with the <sup>133</sup>Cs NMR behavior<sup>17</sup> and the magnetic susceptibility of samples with this thermal history.

**$\text{Cs}^+(\text{18C6})_2\text{Na}^-$ .** As indicated above,  $\text{Cs}^+(\text{18C6})_2\text{Na}^-$  is isostructural with  $\text{Cs}^+(\text{18C6})_2\text{e}^-$ ; each anion is surrounded by eight nearest-neighbor complexed cations. The X-band EPR spectrum of  $\text{Cs}^+(\text{18C6})_2\text{Na}^-$  at 133 K is shown in Figure 5. It exhibits the three signals that have been previously reported for this compound: a main broad peak, a minor broad peak, and a narrow central peak.<sup>3</sup> The relative intensities of three peaks at X-band change from sample to sample. For the sample used in the present work, the intensity ratio of the narrow peak to the main broad peak observed in the X-band spectrum was very small (approximately 0.02), and the minor broad peak was nearly absent. The  $g$ -values of the broad peak and the narrow peak at X-band are 2.0022 and 2.0023, respectively, and no resolved hyperfine splitting was observed. The narrow peak probably arises from itinerant electrons and is exchange-narrowed. The major, somewhat broader peak most likely results from trapped electrons that interact with surrounding hydrogens and complexed cesium

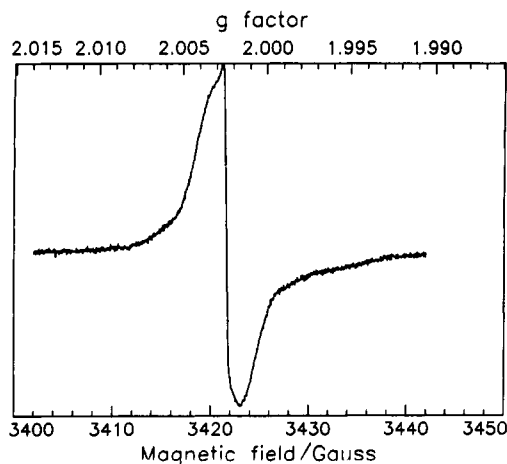


Figure 5. Experimental X-band EPR spectrum of  $\text{Cs}^+(\text{18C6})_2\text{Na}^-$  at 133 K.

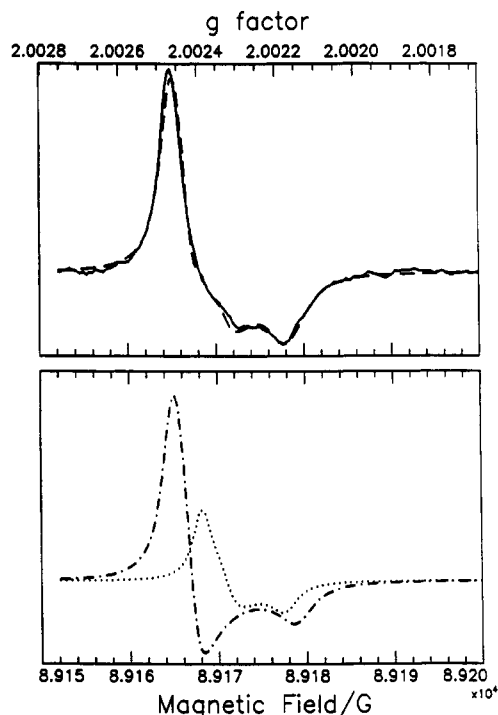


Figure 6. (A, Top) Experimental 250-GHz EPR spectrum of  $\text{Cs}^+(\text{18C6})_2\text{Na}^-$  at 188 K (solid line) and least-squares spectral simulation for two sites with  $g$ -anisotropy (dashed line). (B, Bottom) Individual spectra for the sum spectrum shown in (A). Parameters used for the simulations appear in Table I.

cations, with the linewidth reflecting superhyperfine coupling between the electron and a large number of surrounding nuclei. The presence of three signals shows that several different trapping sites are present in  $\text{Cs}^+(\text{18C6})_2\text{Na}^-$  and that the trapped electrons are isolated from each other. The  $g$ -values are all close to the free electron value, again indicating that the spin-orbit interaction experienced by the electrons is very small.

The X-band EPR intensity of the major signal in  $\text{Cs}^+(\text{18C6})_2\text{Na}^-$  increases linearly with inverse temperature with a nearly zero intercept, showing that the spin susceptibility of the trapped electron in  $\text{Cs}^+(\text{18C6})_2\text{Na}^-$  follows the Curie law.<sup>3</sup> This result indicates the absence of any significant electronic interaction that could produce spin-pairing over this temperature range. The lineshape and linewidth are independent of temperature in the range 130–250 K.

The 250-GHz EPR spectrum of  $\text{Cs}^+(\text{18C6})_2\text{Na}^-$  at 188 K is shown in Figure 6. The sample exhibited no polycrystalline effects such as those observed for the analogous electride. The overall width of the sodide spectrum is comparable to, but slightly

narrower than, that of the electride, and it lacks the sharp feature on the high-field side of the spectrum that is observed for the electride (cf. Figure 2). Nevertheless, the spectrum could not be satisfactorily simulated by using a single electron site with  $g$ -anisotropy and required the assumption of two sites with relative intensities of 3.2:1 to reproduce the details of the experimental line shape, as shown in Figure 6. The  $g$ -tensor for the major signal from  $\text{Cs}^+(\text{18C6})_2\text{Na}^-$  is nearly identical with that of the major signal from the isostructural electride (cf. Table I), providing a strong indication that the two signals correspond to the same trapping site in the crystal lattice. This signal most likely arises from F-center electrons trapped at anionic vacancies.

Direct comparison of the experimental X-band spectrum with a spectral simulation using the  $g$ -tensors measured at the 250-GHz spectrum was not very useful in the case of  $\text{Cs}^+(\text{18C6})_2\text{Na}^-$ . At X-band the  $g$ -anisotropy is so small that any spectral features due to  $g$ -anisotropy are obscured by the linewidth. However, the gross features of the 250-GHz spectrum, including the linewidths, are consistent with the main peak observed at X-band. In addition, the linewidths observed at the two frequencies are quite comparable, consistent with the assignment of this linewidth to a distribution of superhyperfine interactions, which should be frequency-independent.

Comparison of the X-band signals from  $\text{Cs}^+(\text{18C6})_2\text{Na}^-$  and  $\text{Cs}^+(\text{18C6})_2\text{e}^-$  corroborates the conclusion that the trapped electrons are more mobile in the latter compound. If the major trapping site in these two crystals is the same, as indicated by the  $g$ -tensors measured at 250 GHz, the spectrum of the trapped electrons in the electride should also be broadened by interactions with the nuclei at the trapping site and exhibit a similar linewidth. However, the X-band spectrum is significantly narrower than that from the sodide. This result is consistent with the presence of a small amount of spin exchange in the electride, sufficient to average the inhomogeneous width due to the superhyperfine interactions.

The identity of the second electron trapping site implied by the 250-GHz spectrum remains unclear. Most likely, it is contained within the major peak observed at X-band, since it does not appear to correspond to either of the other EPR signals in the X-band spectrum. The spin concentration responsible for the central narrow peak in the X-band spectrum was probably too small to yield a detectable peak at 250 GHz in the sample used, whereas the weak broad peak observed at X-band would be much broader than the experimental 250-GHz spectrum if the linewidth is attributed to  $g$ -anisotropy.

The saturation curve at X-band for  $\text{Cs}^+(\text{18C6})_2\text{Na}^-$  shown in Figure 4B does not reach a maximum in the range 0–0.1 W. According to eq 3, the maximum of the saturation curve corresponds to  $B_1 = \gamma_e(2T_1T_2)^{-1/2}$ , which allows only the estimate of an upper bound for  $T_{1e}$  of  $6 \times 10^{-6}$  s and supports the assumption that the linewidth originates from unresolved hyperfine spin packets.

$\text{Cs}^+(\text{18C6})_2\text{Cs}^-$ . The crystal structure of  $\text{Cs}^+(\text{18C6})_2\text{Cs}^-$  shows that there are seven complexed cesium cations around each  $\text{Cs}^-$  ion at distances of 8.09–9.65 Å.<sup>25</sup> Both cations and anions form zigzag chains parallel to the  $b$ -axis with uniform interionic distances of 8.78 and 8.86 Å, respectively. Each cesium anion is 8.12 Å from another cesium anion in an adjacent chain. Thus, the cesium anions are relatively isolated from one another and from the cesium cations.

Previous X-band EPR spectra of polycrystalline  $\text{Cs}^+(\text{18C6})_2\text{Cs}^-$  showed two overlapping signals.<sup>6</sup> One was a narrow peak (0.62 G) near the free electron  $g$ -value with no appreciable anisotropy; the other was a slightly broader peak that exhibited anisotropy as demonstrated by the spectrum of a single crystal at different orientations.

For the present work,  $\text{Cs}^+(\text{18C6})_2\text{Cs}^-$  samples obtained from different syntheses were used for the X-band and 250-GHz studies.

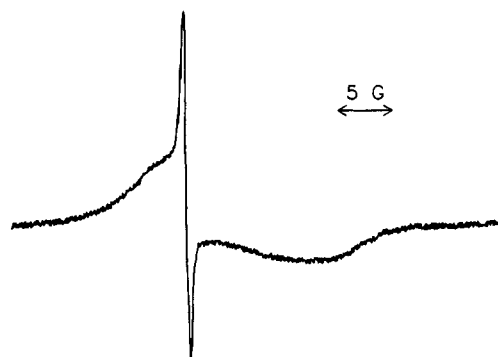


**Figure 7.** Experimental X-band EPR spectrum of  $\text{Cs}^+(\text{18C6})_2\text{Cs}^-$  at 138 K.

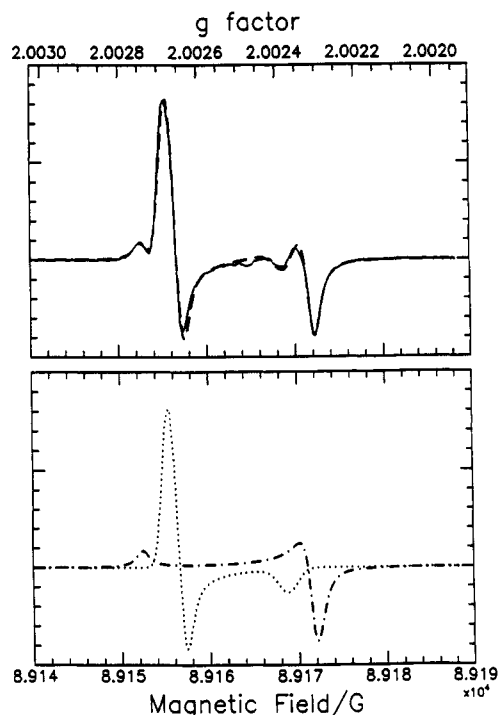


**Figure 8.** (A, Top) Experimental 250-GHz EPR spectrum of  $\text{Cs}^+(\text{18C6})_2\text{Cs}^-$  at 198 K (solid line) and least-squares spectral simulation for two sites with  $g$ -anisotropy (dashed line). (B, Bottom) Individual spectra for the sum spectrum shown in (A). Parameters used for the simulations appear in Table I.

Relatively large crystals were grown and crushed to prepare the sample for the high-frequency EPR, while a polycrystalline sample was used for the X-band studies. The X-band EPR spectrum of polycrystalline  $\text{Cs}^+(\text{18C6})_2\text{Cs}^-$  shown in Figure 7 also shows a broad peak with apparent magnetic anisotropy that accounts for most of the spectral intensity and a central narrow feature qualitatively similar to those previously observed at X-band.<sup>6</sup> The derivative peak-to-peak linewidths of the broad peak and the narrow peak at X-band are 15.1 and 0.64 G, and the average  $g$ -values are 1.9987 and 2.0020, respectively.

The 250-GHz EPR spectrum of  $\text{Cs}^+(\text{18C6})_2\text{Cs}^-$  at 198 K is shown in Figure 8. Although the linewidth of the spectrum is significantly smaller than that of either the sodide or the chloride at high frequency, there was no evidence of any polycrystalline effects. Because of the narrow linewidth, two sites present in a ratio of 1:1 could clearly be resolved from the spectrum. By analogy with the chloride spectrum at 250 GHz, the ceside spectrum consists of two species, each with nearly axial symmetry, situated such that one has its "effective"  $g_{\perp} > g_{\parallel}$ , and one has  $g_{\perp} < g_{\parallel}$ , with  $g_{\perp}$  of each species close to  $g_{\parallel}$  of the other. This can be seen more clearly from the individual site spectra plotted in Figure 8B. There is evidence for another very minor component in the 250-GHz spectrum that appears as a small structure in the center

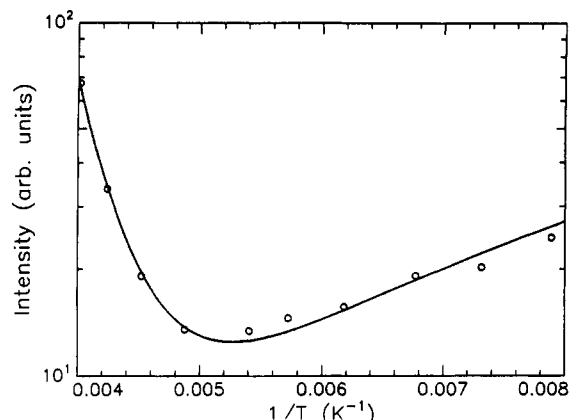


**Figure 9.** Integrated intensity of the X-band EPR spectrum of  $\text{Cs}^+(\text{18C6})_2\text{Cs}^-$  as a function of temperature. The curve represents the least-squares fit of the sum of two functions with exponential and linear (Curie-law) dependence on inverse temperature.

of the spectrum (as distinct from the sharp features produced by polycrystalline effects), but there was insufficient resolution to attempt to characterize this component any further.

Comparison of the X-band and 250-GHz spectra of  $\text{Cs}^+(\text{18C6})_2\text{Cs}^-$  shows that the two components resolved at high frequency correspond most closely to the small narrow line observed in the X-band spectrum. As in the sodide, the linewidth at X-band hampers full resolution of  $g$ -anisotropy, although some anisotropy is apparent in spectra obtained from a single crystal at different orientations.<sup>6</sup> The complete resolution of the powder pattern "turning points" at high frequency is consistent with the X-band single-crystal results and demonstrates that the orientation dependence arises from  $g$ -factor anisotropy instead of hyperfine splitting by  $\text{Cs}^+$  as previously suggested. The overall linewidth at X-band was smaller than the linewidths obtained from the high-frequency spectra (cf. Table I). Reasonable agreement between the narrow peak in the experimental X-band spectrum and the high-field results could be achieved when the linewidths in the X-band simulation were reduced by a factor of 3 relative to the 250-GHz linewidths. There was insufficient resolution to permit the linewidth tensors to be uniquely determined at X-band.

The temperature dependence of the integrated intensity of the X-band spectrum of  $\text{Cs}^+(\text{18C6})_2\text{Cs}^-$  (including both peaks shown in Figure 7) is depicted in Figure 9. The intensity increases with increasing temperature from 200 to 250 K, while below 200 K the temperature dependence follows Curie-law behavior. The solid line shown in Figure 9 represents the least-squares fit to the intensity vs temperature data, utilizing a function of the form

$$I(T) = I_0 \exp\left(-\frac{\Delta E}{kT}\right) + \frac{A}{T} \quad (4)$$

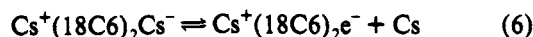
which yielded an apparent  $\Delta E$  of  $0.20 \pm 0.05$  eV. The unusual temperature behavior indicates that additional unpaired spins are produced by an activated process. Since the relative intensities of the two signals observed at X-band are the same over the temperature range studied, it appears that both signals are formed by such a process. One possible mechanism for the production of additional electron spins is the dissociation of spin-paired electrons above 200 K according to the equation



where,  $e_a^-$ , and  $e_i^-$  represent trapped electrons at F-centers and interstitial sites, respectively. At lower temperatures, the rate of this process could be too slow to affect the unpaired electron concentration, and Curie-law behavior would predominate.

Another possible explanation is that there might be a partial composition change as the temperature is increased above 200

K, according to



This reaction would result in an increase of the EPR intensity at higher temperatures and is consistent with previous results<sup>6</sup> from optical spectroscopy of films of  $\text{Cs}^+(18\text{C}6)_2\text{Cs}^-$ .

### Conclusions

Combined EPR studies at 9 and 250 GHz have been carried out on the series of compounds  $\text{Cs}^+(18\text{C}6)_2\text{X}^-$ , where  $\text{X}^- = \text{e}^-$ ,  $\text{Na}^-$ , or  $\text{Cs}^-$ . In all three cases the extremely high  $g$ -factor resolution available at the higher frequency has permitted the resolution of previously undetected species. The major EPR signals from  $\text{Cs}^+(18\text{C}6)_2\text{e}^-$  and  $\text{Cs}^+(18\text{C}6)_2\text{Na}^-$  and the signals from  $\text{Cs}^+(18\text{C}6)_2\text{Cs}^-$  arise from electrons trapped at anion vacancies in the crystal lattice. Comparison of spectra from the electride at the two frequencies shows that the electrons are somewhat mobile, with an effective electron exchange rate less than about  $1 \times 10^7 \text{ s}^{-1}$ . In both alkalides, there is evidence for superhyperfine interaction of the trapped electron with a number of surrounding nuclei, but, as anticipated for the trapped electron in the rather isolated anion vacancies, there is no strong coupling to one or a few nuclei. The  $g$ -factor anisotropies revealed in the high-frequency spectra of all three species are in general consistent with the nonspherical shape of the cavities in the crystal lattice structure as determined by X-ray diffraction, and they suggest that the ground states of the trapped electrons are not strictly describable as S states.

In the alkalides, there are other trapping sites than the F-center, but their nature cannot be deduced from the EPR spectra. The temperature dependence of the EPR intensities for  $\text{Cs}^+(18\text{C}6)_2\text{Cs}^-$  shows that a common spin-paired species can dissociate as the temperature is raised to increase the EPR intensities of both signals.

**Acknowledgment.** This research was supported by the National Science Foundation Solid State Chemistry Grant DMR 90-17292, NSF Chemical Sciences Grant CHE 90-04552, the Michigan State University Center for Fundamental Materials Research, and the Cornell University Materials Science Center. Devel-

opment of the 250-GHz spectrometer was supported by the National Institutes of Health Grant GM-25862 and NSF Grant CHE-90-04552. We are grateful to Dr. John McCracken for assistance with pulsed EPR studies.

### References and Notes

- (1) Dye, J. L.; Ceraso, J. M.; Lok, M. T.; Barnett, B. L.; Tehan, F. J. *J. Am. Chem. Soc.* **1974**, *96*, 608.
- (2) Tehan, F. J.; Barnett, B. L.; Dye, J. L. *J. Am. Chem. Soc.* **1974**, *96*, 7203.
- (3) Shin, D. H.; DeBacker, M. G.; Ellaboudy, A. S.; Dye, J. L. *J. Phys. Chem.* **1991**, *95*, 7085.
- (4) Ellaboudy, A. S.; Bender, C. J.; Kim, J.; Shin, D. H.; Kuchenmeister, M. E.; Babcock, G. T.; Dye, J. L. *J. Am. Chem. Soc.* **1991**, *113*, 1605.
- (5) McCracken, J.; Shin, D.-H.; Dye, J. L. *Appl. Magn. Reson.* **1992**, *3*, 305.
- (6) Issa, D.; Ellaboudy, A. S.; Janakiraman, R.; Dye, J. L. *J. Phys. Chem.* **1984**, *88*, 3847.
- (7) Ellaboudy, A. S.; Dye, J. L.; Smith, P. B. *J. Am. Chem. Soc.* **1983**, *105*, 6490.
- (8) Dawes, S. B.; Ward, D. L.; Huang, R. H.; Dye, J. L. *J. Am. Chem. Soc.* **1986**, *108*, 3534.
- (9) Dye, J. L.; DeBacker, M. G. *Annu. Rev. Phys. Chem.* **1987**, *38*, 271.
- (10) Dye, J. L. In *Valency, The Robert A. Welch Foundation Conference on Chemical Research XXXII* **1988**, 65.
- (11) Dawes, S. B.; Ward, D. L.; Fussa-Rydel, O.; Huang, R. H.; Dye, J. L. *Inorg. Chem.* **1989**, *28*, 2132.
- (12) Dye, J. L. *Science* **1990**, *247*, 663.
- (13) Dye, J. L.; Huang, R. H. *Chem. Br.* **1990**, *26*, 239.
- (14) Dawes, S. B.; Eglin, J. L.; Moeggenborg, K. J.; Kim, J.; Dye, J. L. *J. Am. Chem. Soc.* **1991**, *113*, 1605.
- (15) Moeggenborg, K. J.; Papaioannou, J.; Dye, J. L. *Chem. Mater.* **1991**, *3*, 514.
- (16) Wagner, M. J.; Dye, J. L. Unpublished results, this laboratory.
- (17) Dawes, S. B.; Ellaboudy, A. S.; Dye, J. L. *J. Am. Chem. Soc.* **1987**, *109*, 3508.
- (18) Dye, J. L. *J. Phys. Chem.* **1984**, *88*, 3842.
- (19) Lynch, W. B.; Earle, K. A.; Freed, J. H. *Rev. Sci. Instrum.* **1988**, *59*(8), 1345.
- (20) Bruno, G. V. *Ph.D. Dissertation*, Cornell University, **1973**, p 554.
- (21) Budil, D. E.; Earle, K. A.; Lynch, W. B.; Freed, J. H. *Advanced EPR: Applications in Biology and Biochemistry*; Hoff, A. J., Ed.; Elsevier: Amsterdam, **1989**; Chapter 8.
- (22) GENPLOT program, Computer Graphic Service, Ltd., Ithaca, NY, **1990**.
- (23) Bevington, P. R. *Data Reduction and Error Analysis for the Physical Sciences*; McGraw Hill: New York, **1969**; Chapter 11.
- (24) Poole, C. P. *Electron Spin Resonance*, 2nd ed.; John Wiley & Sons: New York, **1983**; p 590.
- (25) Huang, R. H.; Ward, D. L.; Kuchenmeister, M. E.; Dye, J. L. *J. Am. Chem. Soc.* **1987**, *109*, 5561.